

ON THE ANISOTROPY OF NUCLEI MID-INFRARED RADIATION IN NEARBY ACTIVE GALACTIC NUCLEI

HUAN YANG, JUNXIAN WANG AND TENG LIU

CAS Key Laboratory for Research in Galaxies and Cosmology, Astronomy Department, University of Science and Technology of China, Hefei, Anhui 230026, China; yanghuan@mail.ustc.edu.cn; jxw@ustc.edu.cn; liuteng@ustc.edu.cn

Draft version May 11, 2018

ABSTRACT

In the center of active galactic nuclei (AGNs), the dusty torus absorb the radiation from the central engine and re-emit in mid-infrared (MIR). Observations have detected moderate anisotropy in the dust MIR emission, in the way that type 1 AGNs (type1s) are mildly brighter in MIR comparing with type 2 sources (type2s). However, type1s and type2s were found to follow statistically the same tight MIR – hard X-ray correlation, suggesting the MIR emission is highly isotropic assuming the hard X-ray radiation is inclination independent. We argue this discrepancy could be solved considering the hard X-ray emission in AGN is also mildly anisotropic as we recently discovered. To verify this diagram, we compare the sub-arcsecond $12\mu\text{m}$ flux densities of type1s and type2s using [O IV] $\lambda 25.89\mu\text{m}$ emission line as an isotropic luminosity indicator. We find that on average type1s are brighter in nuclei $12\mu\text{m}$ radiation by a factor of 2.6 ± 0.6 than type2s at given [O IV] $\lambda 25.89\mu\text{m}$ luminosities, confirming the mild anisotropy of the nuclei $12\mu\text{m}$ emission. We show that the anisotropy of the $12\mu\text{m}$ emission we detected is in good agreement with radiative transfer models of clumpy torus. The fact that type 1 and type 2 AGNs follow the same tight MIR – hard X-ray correlation instead supports that both the MIR and hard X-ray emission in AGNs are mildly anisotropic.

Subject headings: galaxies: active — galaxies: nuclei — galaxies: Seyfert — infrared: galaxies

1. INTRODUCTION

In the central a few tens parsecs of active galactic nuclei (AGN), the supermassive black holes are fueled by a lot of gas and dust (see review by Alexander & Hickox 2012). The dusty clouds obscure a significant fraction of the sky of the central engines, and re-emit the absorbed energy mainly in mid-infrared (MIR). MIR observation therefore provides a powerful approach to infer the currently unclear geometric and physical properties of the dusty structure. Due to the angular momentum, the dusty gas likely forms a geometrically and optically thick torus. Popular models include the so-called homogeneous torus model (e.g. Pier & Krolik 1992; Granato et al. 1997), and the clumpy torus model (e.g. Krolik & Begelman 1988; Nenkova et al. 2008a,b; Hönig & Kishimoto 2010).

According to the unification scheme (Antonucci 1993), type 1 and type 2 AGNs (hereafter type1s and type2s) are believed viewed along different inclination angles respect to the torus. As various torus models predict different levels of anisotropy in MIR emission from the torus, comparing the MIR radiation in type1s and type2s therefore could distinguish these models. It turns out that the homogenous torus model is disfavored since the MIR spectral energy distributions (SEDs) of type1s and type2s generally show only mild difference, much weaker than expected from the homogenous torus model (e.g. Alonso-Herrero et al. 2003; Hao et al. 2007; Wu et al. 2009; Tommasin et al. 2010; Ramos Almeida et al. 2011). Furthermore, these MIR spectra and SEDs are well fitted by the clumpy torus models which instead predict low to moderate level of anisotropy in MIR emission (Mason et al. 2006; Nenkova et al. 2008b; Mor et al. 2009; Thompson et al. 2009; Nikutta et al. 2009; Ramos Almeida et al. 2009; Hönig & Kishimoto 2010; Alonso-Herrero et al. 2011; Lira et al. 2013).

Quantifying the anisotropy in MIR observationally is essential to constrain the physical parameters of the torus models (e.g. Levenson et al. 2009; Hönig et al. 2010). Heckman

(1995) reported that the average ratio of $10.6\mu\text{m}$ to 1.4 GHz radio flux densities in type1s is larger by a factor of ~ 4.0 than in type2s. Similarly, Buchanan et al. (2006) explored the MIR anisotropy in Seyfert galaxies with Spitzer spectra after normalizing to 8.4 GHz radio emission. They found type1s are brighter than type2s by a factor of ~ 7 at $5\mu\text{m}$, and the factor of the difference gradually drops to ~ 2 at $35\mu\text{m}$. These studies suggest mild anisotropy of the MIR radiation in Seyfert galaxies, as the optical thin radio emission is believed an isotropic indicator of the intrinsic AGNs accretion power (e.g. Diamond-Stanic et al. 2009).

However, type 1 and type 2 AGNs appear to follow statistically the same tight MIR – X-ray correlation (Lutz et al. 2004; Horst et al. 2006; Gandhi et al. 2009; Levenson et al. 2009; Hönig et al. 2010; Asmus et al. 2013), suggesting the MIR emission is highly isotropic assuming the hard X-ray emission in AGNs is inclination independent. In this case, only tight upper limit to the anisotropy of MIR emission can be obtained, even with a rather large AGN sample containing 155 sources (Asmus et al. 2013), contrary to the studies above which show that MIR emission is mildly anisotropic.

We argue this discrepancy is due to that the hard X-ray emission in AGNs is also mildly anisotropic. Adopting [O IV] $\lambda 25.89\mu\text{m}$ emission line as an isotropic AGN luminosity indicator (Diamond-Stanic et al. 2009; Meléndez et al. 2008; Rigby et al. 2009; Liu & Wang 2010), Liu et al. (2014, hereafter paper I) found both absorption corrected 2 – 10 keV and SWIFT BAT 14 – 195 keV emission in Compton-thin type2s are weaker than in type1s by a factor of $2 \sim 3$. This indicates the hard X-ray radiation in radio quiet AGNs is anisotropic, likely due to the beaming effect of an outflowing X-ray emitting corona. Therefore, hard X-ray emission is likely not a good option to quantifying the moderate anisotropy in MIR emission in AGNs. In this work for the first time we utilize the [O IV] $\lambda 25.89\mu\text{m}$ emission line as the intrinsic luminosity proxy to measure the anisotropy of MIR $12\mu\text{m}$ emission in nearby AGNs.

2. THE SAMPLE

In Paper I, we have compiled a large sample of radio quiet AGNs with [O IV] $\lambda 25.89\mu\text{m}$ line fluxes measured by Spitzer Infrared Spectrometer from five major samples in literature (Diamond-Stanic et al. 2009; Weaver et al. 2010; Tommasin et al. 2010; Dasyra et al. 2009; Pereira-Santaella et al. 2010). We match the [O IV] $\lambda 25.89\mu\text{m}$ catalog to the largest local AGN MIR photometry catalog (Asmus et al. 2014). Asmus et al. (2014) used all available sub-arcsecond resolution MIR imaging and measured the unresolved nuclear fluxes instead of aperture fluxes to minimize the contribution of possible extended emission. Since our scientific goal is to study the MIR emission in typical AGNs, all LINERs in the sample were dropped. As the jet in radio loud AGNs can contribute to MIR radiation, we also excluded known radio loud sources. The final sample includes 34 type 1 AGNs (including Seyfert 1, Seyfert 1.2 and Seyfert 1.5 galaxies, and a couple of type 1 quasars) and 47 type 2 AGNs (including Seyfert 1.8, Seyfert 1.9 and Seyfert 2) that have both [O IV] $\lambda 25.89\mu\text{m}$ and $12\mu\text{m}$ luminosities. We note that dropping the quasars from our sample does not alter the results presented in this work.

The typical resolution of the $12\mu\text{m}$ imaging observations is $0.3''$ (Asmus et al. 2014). As the mean distance in log space is 82 (38) Mpc for type1s (type2s), with 1σ scatter 0.5 (0.4) dex, the mean size of region probed by $12\mu\text{m}$ imaging is 119 (56) parsecs for type1s (type2s). At region scales about 50–100 parsecs, MIR spectroscopy observations of nearby AGNs show strongly reduced or undetected polycyclic aromatic hydrocarbon (PAH) emission compared to spectroscopy in a few hundreds parsecs to kiloparsecs scales (Gandhi et al. 2009; Hönig et al. 2010; Asmus et al. 2014; Esquej et al. 2014). As PAH emission is an indicator of the nuclear star formation activities, weak PAH emission suggests star formation has limited contribution to $12\mu\text{m}$ emission. Therefore the $12\mu\text{m}$ emission mainly comes from dust in the center of Seyfert galaxies. The final matched sample is shown in Table 1. We note that this sample is neither complete nor homogeneous. Possible bias which may affect the results in this study is discussed in §3.

3. STATISTICAL RESULTS

We first plot the $12\mu\text{m}$ versus [O IV] $\lambda 25.89\mu\text{m}$ luminosity in Fig. 1. We see that the $12\mu\text{m}$ radiation strongly correlates to the [O IV] $\lambda 25.89\mu\text{m}$ for both type1s and type2s. The significance of the correlation, according to the Spearman Rank coefficient ρ , is $\rho = 0.85$ at a null significance level of 1×10^{-23} . An intrinsic flux-flux correlation is also present, with $\rho = 0.61$ at a null significance level of 1×10^{-9} .

However, the $12\mu\text{m}$ emissions at given [O IV] $\lambda 25.89\mu\text{m}$ luminosities are remarkably weaker in type2s than in type1s. To statistically quantifying the difference in the $12\mu\text{m}$ luminosities between type1s and type2s, we first perform a linear fit to the relations on the total sample and subsamples of type1s and type2s, taking [O IV] $\lambda 25.89\mu\text{m}$ as the independent variable. We only consider $12\mu\text{m}$ luminosity uncertainties in the analysis, as only part of the sample have [O IV] $\lambda 25.89\mu\text{m}$ luminosities errors which are rather small (typical error is 5%). The best-fitted lines are:

$$\text{type1s} + \text{type2s}: y = (1.06 \pm 0.07)x - 0.2 \pm 3.0$$

$$\text{type1s}: y = (1.12 \pm 0.11)x - 2.3 \pm 4.5$$

$$\text{type2s}: y = (0.96 \pm 0.08)x + 3.8 \pm 3.3$$

We then perform K-S test on the residuals (data points of $12\mu\text{m}$ luminosities minus the best-fit line of total sample, see Fig. 1) of type1s and type2s. At a confidence level of 99.8%, they are not drawn from the same population. The difference of the average residuals between type1s and type2s is 0.4 dex, thus type1s are brighter in $12\mu\text{m}$ (at given [O IV] $\lambda 25.89\mu\text{m}$ luminosities) by a factor of 2.6 ± 0.6 than type2s, suggesting mild anisotropy in MIR radiation.

We note that the statistical results on the difference between type1s and type2s are not sensitive to the linear-fit approach we utilized. For instance, the orthogonal distance regression yields slightly different correlation slopes in $12\mu\text{m}$ versus [O IV] $\lambda 25.89\mu\text{m}$, but the resulted difference in the relative strength of $12\mu\text{m}$ emission between type1s and type2s remains unchanged, i.e., type1s are brighter in $12\mu\text{m}$ by a factor of 2.6 ± 0.6 than type2s at a confidence level of 99.9%.

Before looking into the underlying physics, we examine whether this difference could be artificial due to possible bias of the analysis. We first consider bias of the [O IV] $\lambda 25.89\mu\text{m}$ sample collection. The sources in the matched sample all have high resolution Spitzer IRS spectra. As type2s in the sample tend to have smaller redshifts/distances than type1s, possible slit loss might have underestimated the [O IV] $\lambda 25.89\mu\text{m}$ fluxes more severely in type2s comparing with type1s, correcting which would instead strengthen the difference we have detected. We refer the readers to §4.2 in Paper I for more and thorough discussions on possible bias and the isotropy of [O IV] $\lambda 25.89\mu\text{m}$.

During the analysis, we have excluded 3 sources (all are type2s) with [O IV] $\lambda 25.89\mu\text{m}$ upper limits and 5 sources (all are type2s) with $12\mu\text{m}$ upper limits. Including these upper limits with survival analysis yields consistent results, i.e., type1s are brighter in $12\mu\text{m}$ by a factor of 2.8 than type2s at a confidence level of 99.95%. We note there are 7 type 1.8 and type 1.9 AGNs in our sample, for which optical classifications may be not robust. Excluding these 7 sources from the sample does not change the results in this work. Simply classifying them as type 1 AGNs yield statistically the same results.

Could the difference between type1s and type2s shown in Fig. 1 be due to star formation contribution to [O IV] $\lambda 25.89\mu\text{m}$ as some works claimed that Seyfert 2 may have higher star formation in their host galaxies (Maiolino et al. 1995; Buchanan et al. 2006; but see Imanishi & Wada 2004)? Comparing with [O III] $\lambda 5007$, [O IV] $\lambda 25.89\mu\text{m}$ emission line has higher ionization potential (54.9 eV) thus is less affected by contamination from star formation in the host galaxy. The contamination to [O IV] $\lambda 25.89\mu\text{m}$ from star formation in the host galaxies is rather weak (Pereira-Santaella et al. 2010) and the [O IV] $\lambda 25.89\mu\text{m}$ in Seyfert galaxies and quasars is generally dominated by the AGN. As shown in Pereira-Santaella et al. (2010) the star formation contribution to [O IV] $\lambda 25.89\mu\text{m}$ is much weaker at higher [O IV] $\lambda 25.89\mu\text{m}$ luminosity and could be significant at $L_{[\text{OIV}]} < 10^{40.2} \text{ erg s}^{-1}$. The fraction of AGNs with $L_{[\text{OIV}]} < 10^{40.2} \text{ erg s}^{-1}$ is 22%. Dropping those sources with $L_{[\text{OIV}]} < 10^{40.2} \text{ erg s}^{-1}$ give statistically similar results: type1s are brighter in $12\mu\text{m}$ by a factor of 3.5 ± 0.9 than type2s at a confidence level of 99.96%. Therefore the result in work can not be explained by possible contamination to [O IV] $\lambda 25.89\mu\text{m}$ from the host galaxies.

Finally, if there is any potential bias which could yield a spurious difference in the relative strength of $12\mu\text{m}$ between type1s and type2s as we observed, we should have

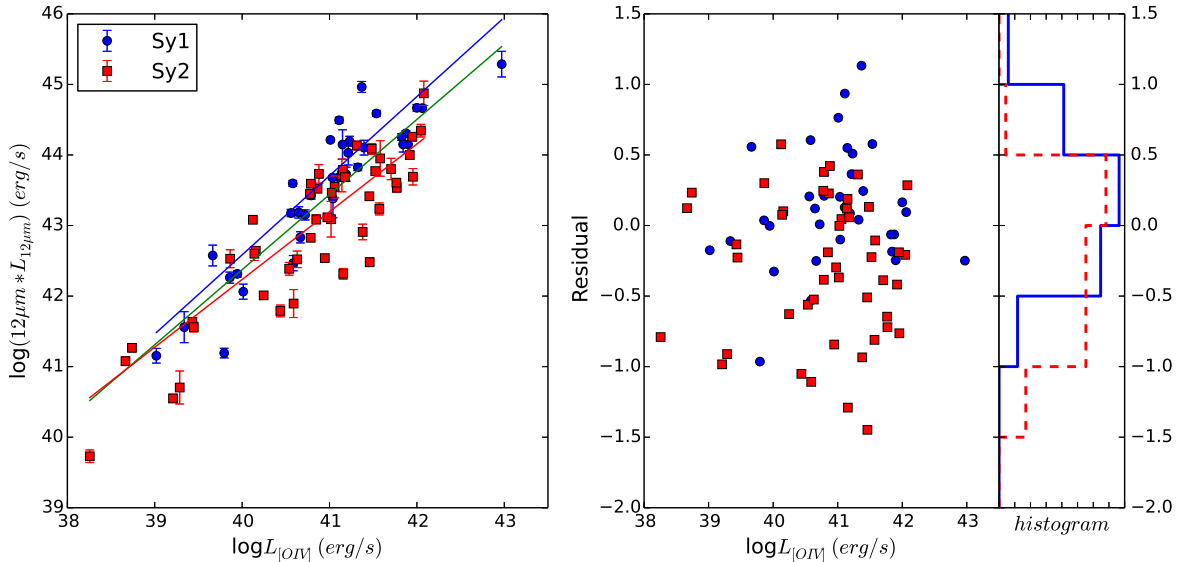


FIG. 1.— Left panel: The relations between [O IV] $\lambda 25.89\mu\text{m}$ and $12\mu\text{m}$ luminosities. Blue dots are type 1 AGNs and red squares are type 2s. The green, blue and red line are best linear fit lines for type 1s + type 2s, type 1s and type 2s respectively. Right panel: Residuals of $12\mu\text{m}$ luminosity data points to the best-fit line of type 1s + type 2s. The histograms show the distributions of residuals for type 1s (blue) and type 2s (red) AGNs respectively. Type 2 AGNs are weaker in $12\mu\text{m}$ luminosities than type 1s.

missed type 1s with relatively weaker $12\mu\text{m}$ emission, and/or type 2s with relatively weaker [O IV] $\lambda 25.89\mu\text{m}$ emission. Bias against sources with relatively brighter emission in one band is unlikely as astronomical observations are generally flux limited. It is however rather puzzling if any such bias works preferentially on type 1s but not type 2s, or vice versa. We conclude that although the sample is not complete or homogeneous, our major results in this work are not affected.

4. DISCUSSION

4.1. Both MIR and X-ray radiation Are Mildly Anisotropic

The mild anisotropy in MIR radiation, as detected in previous studies (Heckman 1995; Buchanan et al. 2006), is confirmed by this work. Particularly, the level of the anisotropy at $12\mu\text{m}$ we detected (by a factor of 2.6) is in good agreement with Fig. 16 in Buchanan et al. (2006) at the same wavelength, which was however based on Spitzer spectra with lower spatial resolution comparing with this work.

Given that the X-ray emission is also mildly anisotropic (Paper I), the mild anisotropy in MIR radiation we detected is also consistent with the picture that type 1s and type 2s follow the same tight correlation between MIR and X-ray intrinsic luminosities (Lutz et al. 2004; Horst et al. 2006; Gandhi et al. 2009; Levenson et al. 2009; Hönig et al. 2010; Asmus et al. 2013).

4.2. Comparing with Clumpy Torus Models

We quantitatively compare our results with two popular radiative transfer modelings of clumpy torus: CLUMPY (Nenkova et al. 2008a,b) and CAT3D (Hönig & Kishimoto 2010). Both models assume thermal equilibrium of dust with radiation of AGNs. The models compute the dust radiation with a range of model parameters (Table 1), including the optical opacity τ_V in V band of each cloud, the torus outer radius Y ($Y = R_{\text{out}}/R_{\text{in}}$, where R_{in} is dust sublimation radius), the average number of clouds along the radial equatorial line N_0 , the power-law index of clouds radial distribution

TABLE 1
PARAMETERS OF CLUMPY TORUS MODELS WE ADOPTED FOR COMPARISON

Parameters	Symbol	CLUMPY	CAT3D
Opacity per single cloud in V band	τ_V	60	50, 80
Torus outer radius $R_{\text{out}}/R_{\text{in}}$	Y	100	150
Clouds along radial equatorial rays	N_0	[2, 15]	[2.5, 10]
Clouds radial distribution r^{-q}	q	[-3, 0]	[-2, 0]
Half covering angle	θ_0	[15°, 60°]	45°

q , and half covering angle θ_0 (see Nenkova et al. 2008b and Hönig & Kishimoto 2010 for more details on the parameters). Both models considered a Gaussian angular distribution of the clouds $N \sim N_0 \exp(-\beta^2/\theta_0^2)$, where θ_0 is the half covering angle, and β is the angle of the line of sight from the equatorial plane. Both models generate SED grids for different sets of those parameters. Using these SED grids, we explore in which region in the parameter space the torus $12\mu\text{m}$ radiation is mildly anisotropic as we observed.

First, to compare emission of torus with different q and N_0 , we take SED grids with parameters set to the model best-fit results of MIR spectra: $\theta_0 = 45^\circ$, $\tau_V = 60$ (50, 80), and $Y = 100$ (150) in CLUMPY (CAT3D) model (Nenkova et al. 2008b; Thompson et al. 2009; Hönig & Kishimoto 2010; Lira et al. 2013), and explore how N_0 and q influence the anisotropy of $12\mu\text{m}$ radiation. In clumpy torus models, the classification as type 1 or type 2 is probabilistic. We use the escape probability defined in Nenkova et al. (2008b) to calculate the average inclination angles of type 1 and type 2 AGNs (escape probability is defined as $\exp(-N_{\text{LOS}})$, while N_{LOS} is the cloud number at the viewing line of sight). For instance, adopting $\theta_0 = 45^\circ$ and $N_0 = 5.0$ (the escape probability is $\exp(-5.0 \exp((\frac{90^\circ - i}{45^\circ})^2))$ where i is the inclination angle), we obtained an average inclination angle of 30° and 60° respectively for type 1 and type 2 AGNs (the escape probabilities at the average inclination angles are 18.4% and 0.1% for

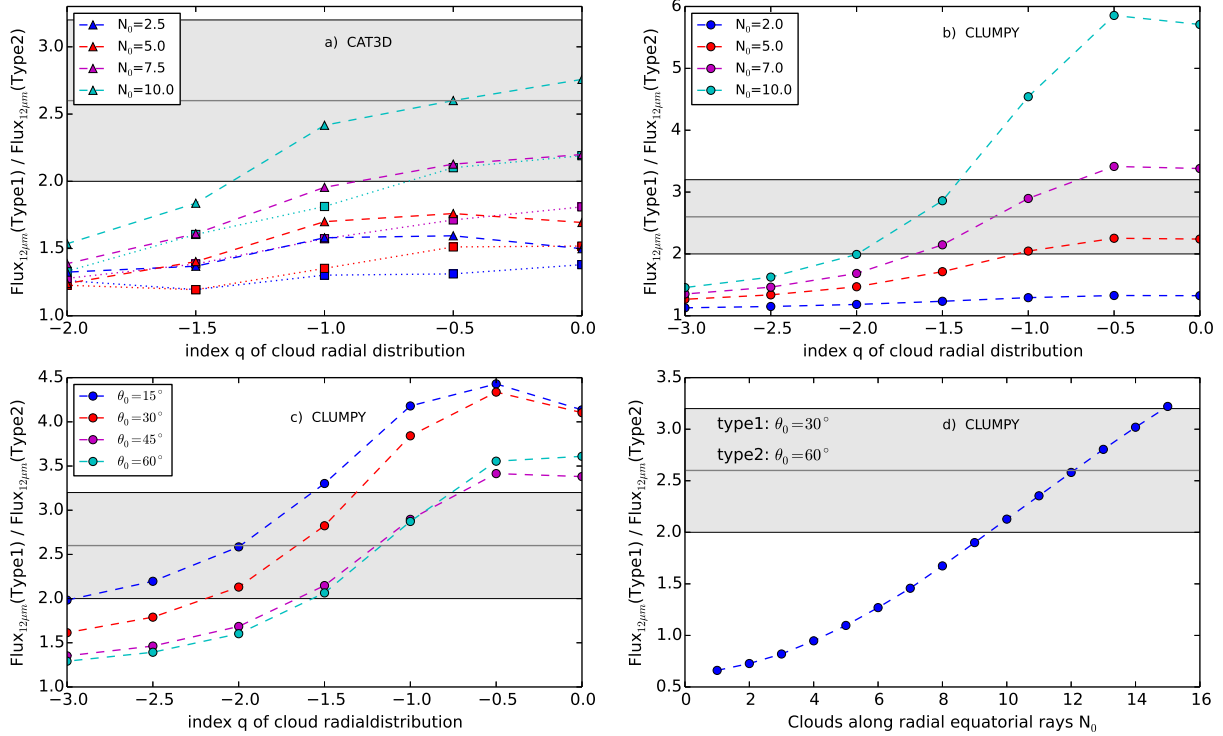


FIG. 2.— a) Flux ratio at $12\mu\text{m}$ of type1s and type2s in clumpy torus model CAT3D for different model parameters. The torus half covering angle θ_0 is fixed at 45° . The dashed line and the triangles show results with $\tau_V=80$. The dotted line and the squares show results with $\tau_V=50$. b) same to a, but using CLUMPY model. c) same to b, but adopting different θ_0 and fixed $N_0 = 7$. d) Assuming different θ_0 for type1s and type2s, but the same viewing angle 50° . q is set to -1.0 . The grey region plot the observed anisotropy of type1s and type2s.

type1s and type2s). We roughly estimate the anisotropy as the ratio of $12\mu\text{m}$ flux viewed at the average inclination angles of type1s and type2s. As shown in Fig. 2, the anisotropy increases when the index of cloud radial distribution q is flatter and the clouds numbers N is larger, consistent with Figure 10 in Nenkov et al. (2008b).

We then explore how the parameter half covering angle θ_0 of the torus affects the anisotropy in dust emission. We adopt CLUMPY SED model as it provides more grids of the physical parameters. We set $N_0 = 7$, $\tau_V = 60$, and $Y = 100$. We compute the average inclination angles of type1s and type2s for different θ_0 and estimate the anisotropy as the ratio of $12\mu\text{m}$ flux viewed at the respective average inclination angle. As shown in Fig. 2c, the anisotropy increases when the half covering angle θ_0 is smaller.

By fitting a sample of AGN SEDs with clumpy torus model, an interesting finding (Ramos Almeida et al. 2011) suggests type 1 and type 2 AGNs have a statistical difference in the half covering angle of the torus, but similar probability distributions of the viewing angles. In this case, we assume different half covering angles for two types ($\theta_0 = 30^\circ$ for type1s and $\theta_0 = 60^\circ$ for type2s), but the same average viewing angle of 50° . We set $q = -1.0$. The result shows that in this scheme, the observed anisotropy could also be reproduced with $N_0 = 10 - 15$. Note that with much smaller N_0 , we would expect opposite anisotropy that type2s are brighter in MIR than type1s, due to its larger covering angle of the dusty torus.

As there is degeneracy among the torus parameters which affect the anisotropy, in this work we are unable to give accurate constraints to individual parameters. The anisotropy

of a factor of ~ 2.6 in dust MIR $12\mu\text{m}$ radiation requires a large N_0 and/or a flat q and/or a small θ_0 . Those parameter ranges are generally consistent with the best-fit results to MIR spectra (Thompson et al. 2009; Hönig & Kishimoto 2010; Lira et al. 2013), particularly Alonso-Herrero et al. (2011) and Ramos Almeida et al. (2011) which include both type 1 and type 2 Seyferts. We conclude that the mild anisotropy we observed in MIR emission is fully consistent with modern clumpy torus models.

4.3. Considering Dust Emission From The Polar Region

Although it is a popular picture that the dust MIR emission in AGNs is dominated by radiation from the clumpy torus, it is challenged by recent MIR interferometric observations. Infrared interferometry observations of 4 nearby AGNs (Circinus, NGC1068, NGC424, NGC3783) at sub-pc resolution suggested that, instead of the torus, the major contributor of MIR emission is dust in the polar region (Tristram et al. 2007; Raban et al. 2009; Hönig et al. 2012, 2013; Tristram et al. 2014). Assuming all AGNs contain polar region dust, the dust emission in polar region will likely dilute the anisotropic emission from the torus.

The level of the dilution is however hard to estimate. The anisotropy of total $12\mu\text{m}$ emission depends on the contribution from both the torus and the polar region. The polar region MIR emission is also likely different between type1s and type2s as the sky coverage of the polar region is likely larger in type1s due to selection effect (Sources with smaller sky coverage of the dusty torus thus larger sky coverage of the polar region are more likely detected as type1s.). This effect may

have played a role in producing the observed MIR anisotropy in AGNs if the polar region component dominate the MIR emission. We note that if type1s have more $12\mu\text{m}$ emission from torus (relative to that from the polar region) than type2s, i.e, the anisotropy in the MIR emission is dominated by the torus but not the polar region, the MIR emission from type1s should appear more compact. Recently, the MIR interferometry observations of a sample of AGNs showed that type1s have a larger fraction of emission concentrated in the central unresolved point sources (Burtscher et al. 2013), which

seems consistent with this diagram.

We thank Daniel Asmus for helpful discussion and comments, and the anonymous referee for valuable suggestions that helped improve the manuscript. This work is supported by Chinese NSF through grant 11233002 & 11421303. JXW acknowledges support from Chinese Top-notch Young Talents Program and National Basic Research Program of China (973 program, grant No. 2015CB857005).

REFERENCES

- Alexander, D. M., & Hickox, R. C. 2012, *NewAR*, 56, 93
- Alonso-Herrero, A., Quillen, A. C., Rieke, G. H., Ivanov, V. D., & Efstathiou, A. 2003, *AJ*, 126, 81
- Alonso-Herrero, A., Ramos Almeida, C., Mason, R., et al. 2011, *ApJ*, 736, 82
- Antonucci, R. 1993, *ARA&A*, 31, 473
- Asmus, D., Honig, S. F., Gandhi, P., Smette, A., & Duschl, W. J. 2014, *MNRAS*, 439, 1648
- Asmus, D., Gandhi, P., Hoenig, S. F., & Smette, A. 2013, *arXiv:1301.3680*
- Buchanan, C. L., Gallimore, J. F., O’Dea, et al. 2006, *AJ*, 132, 401
- Burtscher, L., Meisenheimer, K., Tristram, K. R. W., et al. 2013, *A&A*, 558, A149
- Dasyra, K. M., Yan, L., Helou, G., et al. 2009, *ApJ*, 701, 1123
- Diamond-Stanic, A. M., Rieke, G. H., & Rigby, J. R. 2009, *ApJ*, 698, 623
- Esquej, P., Alonso-Herrero, A., González-Martín, O., et al. 2014, *ApJ*, 780, 86
- Gandhi, P., Horst, H., Smette, A., et al. 2009, *A&A*, 502, 457
- Granato, G. L., Danese, L., & Franceschini, A. 1997, *ApJ*, 486, 147
- Hao, L., Weedman, D. W., Spoon, H. W. W., et al. 2007, *ApJ*, 655, L77
- Heckman, T. M. 1995, *ApJ*, 446, 101
- Hönig, S. F. & Kishimoto, M. 2010, *A&A*, 523, A27
- Hönig, S. F., Kishimoto, M., Antonucci, R., et al. 2012, *ApJ*, 755, 149
- Hönig, S. F., Kishimoto, M., Gandhi, P., et al. 2010, *A&A*, 515, A23
- Hönig, S. F., Kishimoto, M., Tristram, K. R. W., et al. 2013, *ApJ*, 771, 87
- Horst, H., Smette, A., Gandhi, P., & Duschl, W. J. 2006, *A&A*, 457, L17
- Imanishi, M., & Wada, K. 2004, *ApJ*, 617, 214
- Krolik, J. H. & Begelman, M. C. 1988, *ApJ*, 329, 702
- Levenson, N. A., Radomski, J. T., Packham, C., et al. 2009, *ApJ*, 703, 390
- Lira, P., Videla, L., Wu, Y., et al. 2013, *ApJ*, 764, 159
- Liu, T., Wang, J.-X., Yang, H., Zhu, F.-F., & Zhou, Y.-Y. 2014, *ApJ*, 783, 106
- Liu, T. & Wang, J.-X. 2010, *ApJ*, 725, L2831
- Lutz, D., Maiolino, R., Spoon, H. W. W., & Moorwood, A. F. M. 2004, *A&A*, 418, 465
- Maiolino, R., Ruiz, M., Rieke, G. H., & Keller, L. D. 1995, *ApJ*, 446, 561
- Mason, R. E., Geballe, T. R., Packham, C., et al. 2006, *ApJ*, 640, 612
- Mor, R., Netzer, H., & Elitzur, M. 2009, *ApJ*, 705, 298
- Meléndez, M., Kraemer, S. B., Armentrout, B. K., et al. 2008, *ApJ*, 682, 94
- Nenkova, M., Sirocky, M. M., Ivezić, V., & Elitzur, M. 2008a, *ApJ*, 685, 147
- Nenkova, M., Sirocky, M. M., Nikutta, R., Ivezić, V., & Elitzur, M. 2008b, *ApJ*, 685, 160
- Nikutta, R., Elitzur, M., & Lacy, M. 2009, *ApJ*, 707, 1550
- Pereira-Santaella, M., Diamond-Stanic, A. M., Alonso-Herrero, A., & Rieke, G. H. 2010, *ApJ*, 725, 2270
- Pier, E. A. & Krolik, J. H. 1992, *ApJ*, 401, 99
- Planck Collaboration, Ade, P. A. R., Aghanim, N., et al. 2013, *arXiv:1303.5076*
- Raban, D., Jaffe, W., Röttgering, H., Meisenheimer, K., & Tristram, K. R. W. 2009, *MNRAS*, 394, 1325
- Ramos Almeida, C., Levenson, N. A., Rodríguez Espinosa, J. M., et al. 2009, *ApJ*, 702, 1127
- Ramos Almeida, C., Levenson, N. A., Alonso-Herrero, A., et al. 2011, *ApJ*, 731, 92
- Rigby, J. R., Diamond-Stanic, A. M., & Aniano, G. 2009, *ApJ*, 700, 1878
- Ruschel-Dutra, D., Pastoriza, M., Riffel, R., Sales, D. A., & Winge, C. 2014, *MNRAS*, 438, 3434
- Thompson, G. D., Levenson, N. A., Uddin, S. A., & Sirocky, M. M. 2009, *ApJ*, 697, 182
- Tommasin, S., Spinoglio, L., Malkan, M. A., & Fazio, G. 2010, *ApJ*, 709, 1257
- Tristram, K. R. W., Burtscher, L., Jaffe, W., et al. 2014, *A&A*, 563, A82
- Tristram, K. R. W., Meisenheimer, K., Jaffe, W., et al. 2007, *A&A*, 474, 837
- Weaver, K. A., Meléndez, M., Mushotzky, R. F., et al. 2010, *ApJ*, 716, 1151
- Wu, Y., Charmandaris, V., Huang, J., Spinoglio, L., & Tommasin, S. 2009, *ApJ*, 701, 658

TABLE 2
THE SAMPLE

Name	RA (deg.)	DEC (deg.)	Redshift	D (Mpc)	Type	$\log L_{[OIV]}$ (erg s^{-1})	$\log L_{\nu}(12\mu\text{m})$ (erg s^{-1})	error of $\log L_{\nu}(12\mu\text{m})$ (dex)
PG 0026+129	7.30667	13.26750	0.1420	691.0	1.2	42.06	44.66	0.04
I Zw1	13.39558	12.69339	0.0589	269.0	1	41.37	44.96	0.08
NGC 424	17.86512	-38.08347	0.0118	49.5	2	40.88	43.73	0.13
Fairall 9	20.94075	-58.80578	0.0470	215.0	1.2	41.54	44.59	0.04
NGC 526A	20.97662	-35.06553	0.0191	82.8	1.9	41.18	43.69	0.05
Mrk 1014	29.95921	0.39461	0.1631	807.0	1.5	42.97	45.29	0.18
NGC 788	30.27687	-6.81553	0.0136	57.2	2	40.98	43.12	0.05
Mrk 590	33.63983	-0.76669	0.0264	116.0	1	40.58	43.60	0.04
NGC 1068	40.66963	-0.01328	0.0038	14.4	2	41.70	43.80	0.15
NGC 1144	43.80083	-0.18356	0.0288	128.0	2	41.02	43.09	0.25
MCG-2-8-39	45.12746	-11.41572	0.0299	133.0	2	41.48	44.09	0.08
NGC 1194	45.95462	-1.10375	0.0136	58.2	1.9	40.78	43.45	0.04
NGC 1365	53.40154	-36.14039	0.0055	17.9	1.8	40.95	42.54	0.04
NGC 1386	54.19242	-35.99942	0.0029	16.5	2	40.54	42.39	0.09
NGC 1566	65.00175	-54.93781	0.0050	14.3	1.5	39.34	41.56	0.22
NGC 1667	72.15475	-6.31997	0.0152	67.8	2	40.59	41.89	0.20
MCG-1-13-25	72.92283	-3.80925	0.0159	71.2	1.2	39.66	42.57	0.15
ESO 33-2	73.99567	-75.54117	0.0181	82.3	2	41.06	43.55	0.16
Ark 120	79.04758	-0.14983	0.0327	149.0	1	41.01	44.21	0.02
ESO 362-18	79.89917	-32.65758	0.0124	56.5	1.5	40.56	43.18	0.05
IRAS 05189-2524	80.25579	-25.36261	0.0426	196.0	2	42.08	44.87	0.17
ESO 253-3	81.32533	-46.00583	0.0425	196.0	2	42.05	44.34	0.09
NGC 2110	88.04742	-7.45622	0.0078	35.9	2	40.85	43.09	0.06
H0557-385	89.50833	-38.33464	0.0339	156.0	1.2	41.11	44.49	0.04
ESO 5-4	91.42346	-86.63186	0.0062	22.4	2	39.43	41.64	0.05
Mrk 3	93.90150	71.03753	0.0135	60.6	2	41.95	43.69	0.12
PG 0844+349	131.92696	34.75122	0.0640	302.0	1	41.21	44.03	0.17
MCG-1-24-12	140.19271	-8.05614	0.0196	93.8	2	41.03	43.46	0.04
MCG-5-23-16	146.91733	-30.94872	0.0085	42.8	1.9	40.79	43.59	0.04
Mrk 1239	148.07958	-1.61208	0.0199	95.4	1	41.23	44.19	0.07
NGC 3081	149.87308	-22.82628	0.0080	40.9	2	41.38	42.91	0.11
NGC 3227	155.87742	19.86506	0.0039	22.1	1.5	40.59	42.47	0.11
NGC 3281	157.96704	-34.85369	0.0107	52.8	2	41.77	43.61	0.05
NGC 3783	174.75733	-37.73867	0.0097	48.4	1.5	41.03	43.68	0.03
NGC 3982	179.11721	55.12525	0.0037	21.4	2	39.45	41.56	0.07
NGC 4051	180.79004	44.53133	0.0023	12.2	1	39.95	42.31	0.04
NGC 4138	182.37408	43.68531	0.0030	13.8	1.9	38.67	41.08	0.06
NGC 4151	182.63575	39.40572	0.0033	13.3	1.5	40.67	42.83	0.08
NGC 4235	184.29117	7.19158	0.0080	41.2	1.2	39.86	42.26	0.08
NGC 4258	184.73958	47.30397	0.0015	7.6	2	38.74	41.27	0.06
NGC 4388	186.44479	12.66208	0.0084	19.2	2	41.16	42.32	0.08
NGC 4395	186.45358	33.54692	0.0011	4.3	1.8	38.26	39.73	0.09
NGC 4501	187.99650	14.42039	0.0076	17.9	2	39.21	40.55	0.06
NGC 4507	188.90263	-39.90925	0.0118	57.5	2	41.15	43.79	0.04
NGC 4593	189.91429	-5.34425	0.0090	45.6	1	40.72	43.15	0.07
IC 3639	190.22021	-36.75586	0.0109	53.6	2	40.86	43.52	0.04
NGC 4941	196.05475	-5.55161	0.0037	21.2	2	40.25	42.01	0.05
ESO 323-77	196.60887	-40.41467	0.0150	71.8	1.2	41.19	43.73	0.10
NGC 5033	198.36446	36.59394	0.0029	18.1	1.2	39.79	41.19	0.07
MCG-3-34-64	200.60192	-16.72847	0.0165	79.3	2	41.92	44.00	0.05
NGC 5135	201.43358	-29.83367	0.0137	66.0	2	41.57	43.24	0.08
M51a	202.46962	47.19517	0.0015	8.1	2	39.29	40.70	0.23
MCG-6-30-15	203.97379	-34.29553	0.0077	38.8	1.5	40.65	43.19	0.08
NGC 5273	205.53475	35.65422	0.0035	15.3	1.5	39.02	41.15	0.10
IC 4329A	207.33029	-30.30944	0.0161	76.5	1.2	41.87	44.31	0.04
NGC 5347	208.32429	33.49083	0.0078	38.1	2	40.12	43.08	0.04
Circinus	213.29146	-65.33922	0.0014	4.2	2	40.16	42.64	0.05
NGC 5506	213.31204	-3.20758	0.0062	31.6	2	41.46	43.41	0.03
NGC 5548	214.49804	25.13678	0.0172	80.7	1.5	41.04	43.38	0.27
NGC 5643	218.16975	-44.17442	0.0040	20.9	2	40.63	42.52	0.12
NGC 5728	220.59958	-17.25308	0.0094	45.4	2	41.46	42.48	0.06
IC 4518W	224.42158	-43.13211	0.0163	76.1	2	41.77	43.54	0.07
Mrk 841	226.00500	10.43783	0.0364	170.0	1.5	41.90	44.15	0.13
NGC 5995	237.10396	-13.75778	0.0252	117.0	1.9	41.31	44.13	0.06
NGC 6300	259.24779	-62.82056	0.0037	14.3	2	39.86	42.53	0.13
Fairall 49	279.24288	-59.40239	0.0200	90.1	2	41.58	43.95	0.25
ESO 103-35	279.58475	-65.42756	0.0133	59.5	2	41.14	43.71	0.23
Fairall 51	281.22492	-62.36483	0.0142	64.1	1.5	41.11	43.68	0.04
ESO 141-55	290.30892	-58.67031	0.0371	169.0	1.2	41.39	44.10	0.10
NGC 6814	295.66933	-10.32350	0.0052	20.1	1.5	40.01	42.06	0.11
NGC 6860	302.19537	-61.10019	0.0149	65.8	1.5	40.79	43.43	0.05
NGC 6890	304.57542	-44.80672	0.0081	33.8	2	40.14	42.60	0.10
Mrk 509	311.04058	-10.72347	0.0344	153.0	1.5	41.83	44.25	0.05
IC 5063	313.00975	-57.06878	0.0113	49.1	2	41.52	43.77	0.03

TABLE 2 — *Continued*

Name	RA (deg.)	DEC (deg.)	Redshift	D (Mpc)	Type	$\log L_{[\text{OIV}]}$ (erg s^{-1})	$\log L_{\nu}(12\mu\text{m})$ (erg s^{-1})	error of $\log L_{\nu}(12\mu\text{m})$ (dex)
PG 2130+099	323.11588	10.13875	0.0630	288.0	1.5	42.00	44.67	0.05
NGC 7172	330.50787	-31.86967	0.0087	34.8	2	40.78	42.83	0.04
Mrk 304	334.30108	14.23914	0.0658	301.0	1	41.15	44.15	0.21
NGC 7314	338.94246	-26.05047	0.0048	18.3	2	40.44	41.79	0.08
NGC 7469	345.81508	8.87400	0.0163	67.9	1.5	41.32	43.83	0.05
Mrk 926	346.18117	-8.68572	0.0469	210.0	1.5	41.84	44.15	0.11
NGC 7674	351.98633	8.77903	0.0289	126.0	2	41.95	44.26	0.06

NOTE. — (1) Commonly used object names; (2-4) Ra, Dec, redshifts from NED; (5) Distances from Asmus et al. 2014, most of which are redshift-based luminosity distances with $H_0 = 67.3$, $\Omega_m = 0.315$, and $\Omega_{vac} = 0.685$ (Planck Collaboration et al. 2013), plus a few redshift-independent distances; (6) Optical AGN classifications from paper I; (7) Luminosities of [O IV] $\lambda 25.89\mu\text{m}$ from paper I; (8-9) Nuclear sub-arcsecond scale monochromatic luminosities and errors at rest frame $12\mu\text{m}$ (Asmus et al. 2014).